ResearchGate

See discussions, stats, and author profiles for this publication at: https://www.researchgate.net/publication/321170736

Destabilizing the AXH tetramer by intra- and inter-dimer mutations: molecular mechanisms and potential...

Article *in* Biophysical Journal · December 2017

CITATIONS
0

READS
75

6 authors, including:

Umberto Morbiducci
Politecnico di Torino
224 PUBLICATIONS **2,155** CITATIONS
SEE PROFILE

Diana Massai
Politecnico di Torino
63 PUBLICATIONS **335** CITATIONS
SEE PROFILE

Andrea Danani
Dalle Molle Institute for Artificial Intelligence
82 PUBLICATIONS **1,221** CITATIONS
SEE PROFILE

Marco A Deriu
University of Applied Sciences and Arts of Sout...
106 PUBLICATIONS **547** CITATIONS
SEE PROFILE

Some of the authors of this publication are also working on these related projects:

3D Virtual Liver View project

Ion Channel Energetics View project

All content following this page was uploaded by Marco A Deriu on 22 November 2017.

The user has requested enhancement of the downloaded file.

Manuscript – PrePrint Version

Destabilizing the AXH tetramer by intra- and inter-dimer mutations: molecular mechanisms and potential anti-aggregation strategies

Gianvito Grasso[1], Umberto Morbiducci[2], Diana C. Massai[2], Jack A. Tuszynski[3], Andrea Danani[1], and Marco A. Deriu[1]*

[1] Istituto Dalle Molle di studi sull'Intelligenza Artificiale (IDSIA), Scuola universitaria professionale della Svizzera italiana (SUPSI), Università della Svizzera italiana (USI), Centro Galleria 2, Manno, CH-6928, Switzerland.

[2] Department of Mechanical and Aerospace Engineering, Politecnico di Torino, Corso Duca degli Abruzzi 24, IT-10128, Torino, Italy.

[3] Department of Physics, University of Alberta, Edmonton AB, Canada.

[*]corresponding author

Running Title. *Destabilizing AXH tetramer by intra and inter-dimer mutations*

Abstract

The AXH domain of protein Ataxin 1 is thought to play a key role in the misfolding and aggregation pathway responsible for Spinocerebellar ataxia 1. For this reason, a molecular level understanding of AXH oligomerization pathway is crucial to elucidate the aggregation mechanism which is thought to trigger the disease.

The present study employs classical and enhanced molecular dynamics to identify the structural and energetic basis of AXH tetramer stability. Results of the present work elucidate molecular mechanisms behind the destabilizing effect of protein mutations which lately affect the AHX tetramer assembly.

Moreover, results of the study point the attention, for the first time, on R638 protein residue, which shown to play a key role in AXH tetramer stability. Therefore, R638 might be also implicated in AXH oligomerization pathway and stands out as a target for future experimental studies focused on self-association mechanisms and fibril formation of full-length ATX1.

keywords

Neurodegenerative disease, spinocerebellar ataxia, molecular dynamics, AXH domain, metadynamics, free energy landscape, protein-protein interactions, tetramer, principal pomponent analysis, conformational stability.

Introduction

Protein misfolding and aggregation have been recognized as closely related to the onset of several neurodegenerative disorders [1,2] such as polyglutamine (polyQ) diseases, caused by expanded cytosine-adenine-guanine (CAG) repeats encoding a long polyQ tract in the respective proteins. It has been also experimentally demonstrated that structured protein domains far from the polyQ tract play a key role in the pathogenesis [3–6]. A clear example of this mechanism is given by the structured Josephin Domain, that is fundamental in promoting the first step of Ataxin-3 aggregation pathway [7–13], in Spinocerebellar Ataxia Type 3. This is also the case of the misfolding process of Ataxin-1 (ATX1), a polyQ protein responsible for the neurodegenerative disease Spinocerebellar Ataxia Type 1 [1,5]. Despite polyglutamine expansion is an essential step in the disease onset, it is now established that it is the AXH domain of ATX1, so far the only structured globular region identified along the protein sequence, that modulates ATX1 misfolding and aggregation pathway [1,2,14–17]. The observed significant reduction of Ataxin-1 aggregation as a consequence of the replacement of AXH domain with the homologous sequence of the transcription factor HBP1 [15], has demonstrated that the AXH domain is fundamental in driving the ATX1 aggregation mechanism. At the same time, an intrinsic tendency to form fibers in the absence of chemical and/or thermal destabilization was observed in the isolated AXH [15].

Experimental [4,18] and *in silico* [19,20] studies have already highlighted the presence of a well-preserved tertiary and quaternary structure for the AXH domain, apart from the N-terminal (*Nter*) region of each AXH monomer (AXH^{m}), which is involved in the dimer interface. More in detail, the AXH domain is constituted by an asymmetric homo-dimer [5,18] with an interface characterized by 20-residue motifs mutually adapting, although different [4].

A recent study pointed the attention on the conformational fluctuations characterizing the AXH^m in solution [19]. Our results depicted the AXH protein as characterized by a relatively stable structure, except for the *Nter* tail switching between several conformations. Moreover, an in-depth analysis of the AXH monomer-monomer interface highlighted the self-association mode for the AXH dimer. Based on these findings and in accordance with previous experimental observations [18], Grasso and colleagues concluded that the interactions leading to the dimer formation might be able to stabilize the *Nter* region of the AXH, which is in turn involved in the dimeric interface [19].

The main AXH inter-dimer interactions identified in experimental studies [5,18] suggest a protein organization into higher order tetramers. All the previously mentioned tetramer models are very similar in terms of unit cell dimensions, crystal packing, asymmetric unit content, and quaternary and monomeric backbone structures, as demonstrated in recent literature [18]. A number of AXH mutations have been also experimentally tested to identify residues responsible for the destabilization of the monomer/dimer/tetramer equilibrium [18]. In detail, the tetramer population was noticeably reduced by residue I580 mutation, thus identifying the above mentioned residue as a key player in mediating the AXH self-association [18].

However, the AXH self-association mechanism is not yet clarified and several questions remain open. For example, it is unclear how the residue I580, located in the monomer-monomer interface (intra-dimer), is able to drive the tetramer assembly [18]. Unanswered questions like this make of great interest the investigation of non-local molecular effects consequence of single point mutations, and closely related to modifications in AXH self-assembly tendency.

In this study, molecular modeling was applied to fully characterize structural and energetics of the AXH tetramer assembly. Classical and enhanced molecular dynamics (MD) have allowed to

elucidate those non-local molecular events triggered by a protein mutation which lately affect the conformational feature of the whole AHX tetramer assembly. Moreover, first in literature, the free energy landscape associated to the AXH tetramer formation process was estimated in presence of amino acid substitutions. Such a picture of the free energy landscape is crucial for a clear understanding of the molecular processes driving protein assembly and aggregation.

Our data confirm the key role of I580 and suggest R638 as a further residue mainly determining AXH tetramer stability. Outcome of the present work may be of interest for both (1) a better understanding of the self-association mechanism characterizing AXH dimers, and (2) identifying novel modulators of the AXH protein-protein interaction predicted in the present work as important for AXH tetramer stability.

Materials and Methods

Classical Molecular Dynamics on AHX Dimers

The AXH dimer model was extracted from the 4APT [18] model, as in previous studies [19,20]. For consistency with previous literature, residue numbering refers to the UniProtKB/Swiss-Prot entry No. P54253 +1. Here, two different AXH dimer molecular systems were investigated, the wild type AXH dimer (AXHd-WT simulation) and the mutated AXH dimer (AXHd-I580A). Based on recent experimental evidences [21], the alanine mutation on residue I580 was considered. Simulations were carried out by applying the computational scheme described below.

Each AXH dimer was placed in a dodecahedron box where the minimum distance between the protein and the edge of the box was set to 1.2 nm. The box was then fully solvated in explicitly modeled water and the total charge was neutralized by the addition of Cl^- and Na^+ ions. Each dimer system in water consisted of about 40,000 interacting particles. Following an initial energy minimization of 1000 steps of steepest descent, two preliminary position restraint MD simulations

(each one of the duration of 100 ps) were carried out in NVT and NPT ensemble, respectively, where the heavy atoms of the proteins were restrained using a force constant of 1000 kJ $mol^{-1}nm^{-2}$. During the first restrained MD simulation, involving MD in the NVT ensemble, protein and non-protein atoms were coupled separately to temperature baths using a *v-rescale* coupling algorithm [22] with a coupling time of 1 ps. Subsequently, the second restrained MD simulation was performed keeping the pressure at 1 bar by applying Berendsen's weak coupling method [23] with a time constant of 5 ps. Finally, 600 ns of production MD was simulated in NPT ensemble. The *v-rescale* coupling algorithm [22] was applied again to maintain the system's temperature at 310 K (time constant of τ_T=0.1 ps) and the pressure was maintained at 1 bar using the Parrinello-Rahman [24,25] barostat (time constant of τ_P=2ps) in the isobaric-isochoric ensemble with long-range dispersion correction applied for both the energy and pressure terms. AMBER99-ILDN force-field [26,27] and TIP3P model [28] were employed to define the protein topology [26,29] and water molecules, respectively. Gromacs-5.1.2 [30] with the PLUMEDv2.3 patch [31] were employed for MD simulations and data analysis [32]. Conformational stability is reported in Supporting Information (S1.1) Visual Molecular Dynamics (VMD) [33] package was employed for the visual inspection of the simulated systems. The computational data taken from the Classical MD trajectory were analyzed to characterize the AXH dimer-dimer interface. Principal Component Analysis (PCA) was applied to reduce the dimensionality of the system, elucidating large-scale and low-frequency modes, respectively, thus yielding collective motions directly related to a specific molecular event [34]. After the alignment of the AXH^m C-alpha (C_α) Cartesian coordinates, the covariance matrix was calculated and diagonalized.

AHX tetramers free energy landscape estimation

Also in this case, two different AXH tetramer molecular systems (constituted by monomer A, B, C and D) were investigated, the wild type AXH tetramer (AXHt-WT simulation) and the mutated AXH tetramer (AXHt-I580A). The AXH tetramer structure (PDB code 4APT[18]) was fully solvated in a dodecahedron box where the minimum distance between the protein and the edge of the box was set up to 2.5 nm. The total charge was neutralized by the addition of Cl− and Na+ ions. The resulting system placed in water consisted of about 220,000 interacting particles. Classical 300 ns MD equilibration were carried out on both systems, applying the same scheme as for the 4APT dimer models.

Starting from the equilibrated system obtained by classical MD simulation, Metadynamics was applied for the estimation of the dimer-dimer binding free energy. Metadynamics [35,36] is a powerful technique able to enhance sampling in MD simulations by adding a history dependent bias potential on the subspace identified by a set of user-defined Collective Variables (CVs). In detail, Gaussian deposition rate of 0.2 kJ/mol·ps was initially applied on the AXH inter-dimer distance and gradually decreased on the basis of an adaptive scheme. A Gaussian width of 0.2 Å was used following a well-established scheme [37,38]. In particular, the Gaussian width value was of the same order of magnitude as the standard deviation of the distance CV, calculated during unbiased simulations. Each system was simulated (2 fs time step) until convergence was reached. The reconstruction of the free-energy surface was performed by the reweighting algorithm procedure [39], allowing the estimation of the free energy landscape as a function of two CVs : a) distance between dimer AB and dimer CD, and b) the cosine of the angle between vectors connecting the center of mass of two distinct AXH regions per dimer (identified as "*cosine CV*" in the following). Exhaustive details on the definition of the CVs (Supporting Information, S1.2)

and the convergence of the Metadynamics simulations (Supporting Information, S1.3), are presented as Supporting Information.

Results

Wild type and Mutated AXH Molecular Dynamics: Dimer Level

Protein structural stability of systems AXHd-WT and AXHd-I580A was analyzed by monitoring the time evolution of the Root Mean Square Deviation (RMSD). It can be observed that protein conformational stability was satisfactorily reached in the last 100 ns of the simulations (Supporting Information, S1.1). The dimerization interface in both AXH-WT and AXH-I580A simulations buried 14.5 nm^2 of solvent accessible surface, in agreement with previous literature [20]. The application of PCA highlighted the large-scale and low-frequency modes mainly related to a specific protein conformational change. After the alignment of the AXH C-alpha atoms, the covariance matrix was calculated and diagonalized for each system (AXHd-WT and AXHd-I580A).

The MD trajectory of both AXHd-WT and AXHd-I580A system was filtered along the first and second PCA eigenvector. The Root Mean Square Fluctuation was calculated over the filtered MD trajectory (Figure 1a, AXHd-WT system; Figure 1b, AXHd-I580A system) to highlight fluctuations related to major motion modes of the dimer.

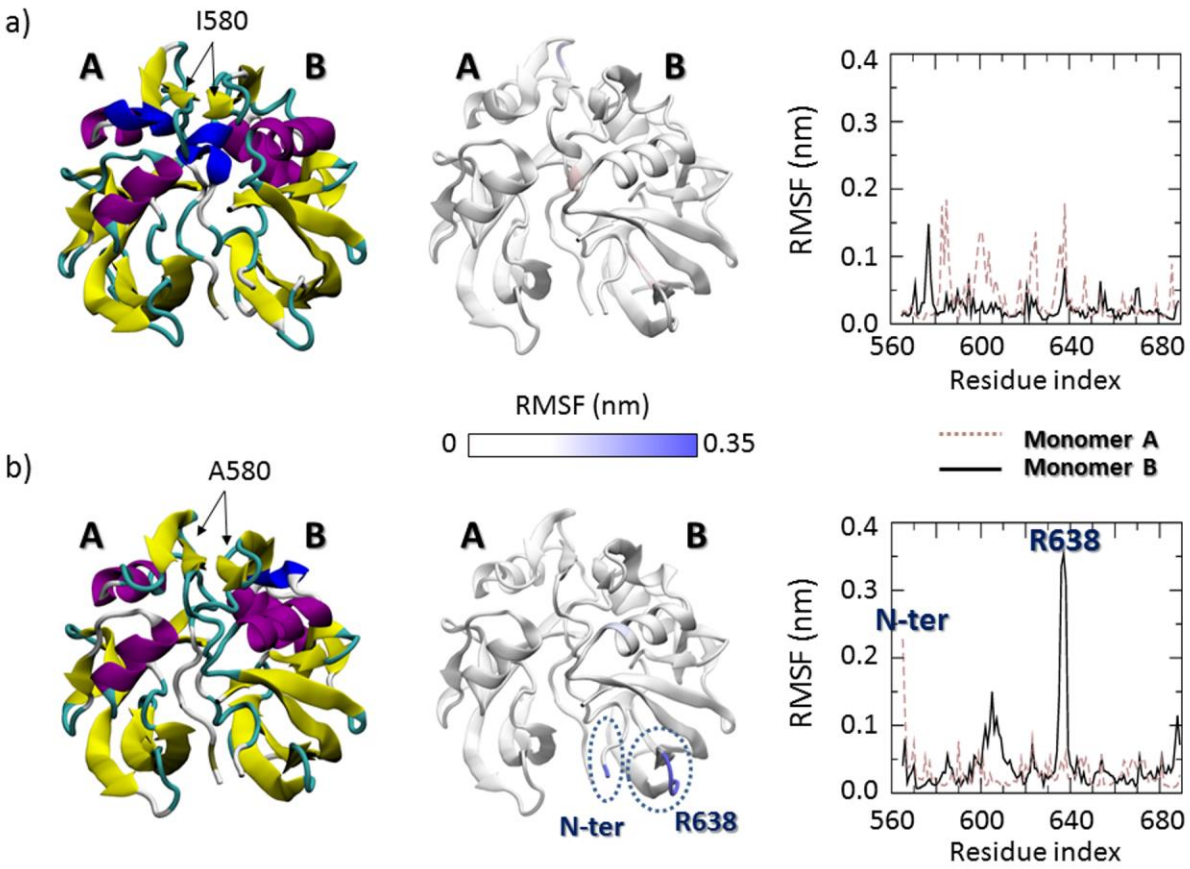

Figure 1. a) Visual inspection of the AXH-WT conformational arrangement at the equilibrium (left). The Root Mean Square Fluctuation (RMSF) is reported in the right panel and represented on the protein 3D structure (center). b) Visual inspection of the AXH-I580A conformational arrangement at the equilibrium (left). The Root Mean Square Fluctuation (RMSF) is reported in the right panel and represented on the protein 3D structure (center).

By comparing the RMSF curves (Figure 1a and Figure 1b, right), it can be noticed that the I580 mutation may lead to a destabilization of the AXH N-terminal tail (AXH d-I580A $RMSF_{Nter}$=0.23 nm, Figure 1b, pink dashed line) on one monomer (e.g., monomer A in Figure 1b). Notably, the RMSF profile of the interacting monomer (Figure 1b, monomer B), is instead characterized by a relevant fluctuation peak of residue R638 (AXHd-I580A $RMSF_{R638}$= ~ 0.35 nm). Interestingly,

the R638 on monomer B is spatially close to the N-terminal tail of monomer A and relatively far from residue I580 (Figure 1). These findings suggest a non-local correlation between residue I580 in one monomer and residue R638 in the interacting one, mediated by the N-terminal tail. In a greater detail, the increased fluctuation of the N-terminal tail, as induced by I580 mutation, drives a conformational modification of residue R638 on the interacting monomer. Interestingly R638 participates to dimer-dimer interaction in AXH tetramerization. Therefore, it is meaningful pointing the attention on the conformational behavior of residue R638 in AXH tetramer dynamics as done in the following.

Wild type and Mutated AXH Molecular Dynamics: Tetramer level

Using the same protein model (PDB code 4APT[18]), two different AXH tetramer systems were considered, the wild type AXH tetramer (AXHt-WT simulation) and the mutated AXH tetramer (AXHt-I580A). Classical 300 ns long MD equilibration was performed on both systems. The two AXH tetramer systems are initially characterized by the same interdimer contact regions: T596-I600, V653-T658 and G680-K689 of monomer B and T596-T615, G635-Q640, V653-T658 and G680-K689 of monomer C. Dimer-dimer conformational arrangement is quite conserved during the AXHt-WT simulation, as also demonstrated by the stable RMSD plot observed from 50 to 300 ns (Figure 2a, top). The previously mentioned arrangement is characterized by residues R638B and R638C non-covalently bound by two hydrogen bonds between the guanidinium group on one residue and the backbone carbonyl oxygen on the other one (Figure 2b-I, Movie-S1). In the AXHt-I580 system hydrogen bonds are lost, weakening the interdimer interaction (Figure 2b-II, Movie-S2).

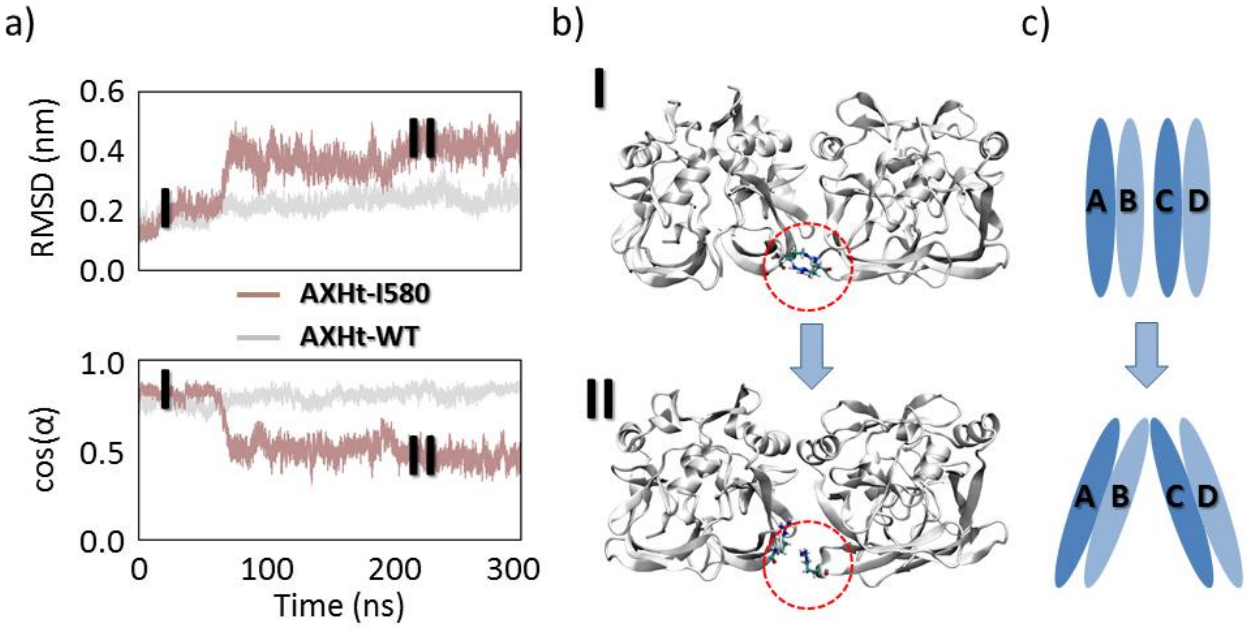

Figure 2. Backbone RMSD throughout the overall MD simulation for wild type (grey) and mutated protein (brown). b) Visual inspection of the molecular systems at the equilibrium in case of AXHt-WT (I) and AXHt-I580A system (II). c) Scheme illustrating the main structural modifications characterized by a relative rotation between dimers AB and CD.

This result is also confirmed by the Radial Distribution Function (RDF) of the guanidinium group amine nitrogen atoms with respect the backbone carbonyl oxygens of the interacting arginine (Figure 3a). The peak at 2.8 Å characterizing the AXHt-WT trajectory (Figure 3a, black curve) does indicate the presence of a strong primary interaction (hydrogen bond) between R638B and R638C. In summary, the I580 mutation destabilizes the protein region containing the R638 residues, as already observed (Figure 1), thus leading to a less stable interaction between R638B and R638C, as highlighted by the RDF analysis (Figure 3a, brown curve). Consequently, it was observed a relative rotation between dimers AB and CD in the AXHt-I580A, inducing a marked decrease of dimer-dimer contact area, when compared to AXHt-WT ($AXHt\text{-}WT_{buried}$=14.7±0.8 nm^2; $AXHt\text{-}I580A_{buried}$=11.9±0.5 nm^2). The rotation between dimers AB and CD can be described

computing the cosine of the angle between vectors connecting the center of mass of two distinct AXH regions per dimer (Figure 2a, bottom).

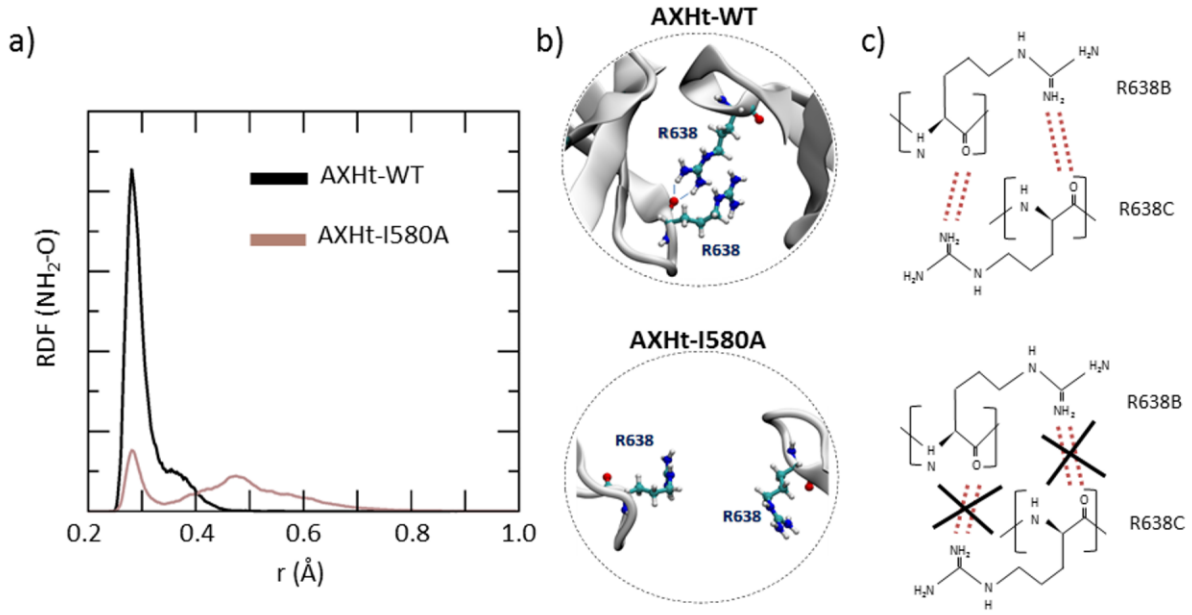

Figure 3. (a) RDF of the amine nitrogen atoms of guanidinium group with respect the backbone carbonyl oxygens of the interacting arginine residue. Only R638B and R638C are considered for the calculation. Two different peaks at 2.8 Å and 4.7 Å can be identified. The first peak is related to the primary interaction resulting from the hydrogen bond between the amine hydrogen atoms and the backbone oxygen, while the second peak indicates the water-mediated hydrogen bonding [57]. The hydrogen bonds between the R638B and R638C residues are also represented in (b) and (c).

Wild type and mutated AXH tetramer free energy landscape and unbinding pathway

Starting from the equilibrated systems obtained by classical MD simulations, the process of dimer-dimer unbinding was investigated by metadynamics. An overall picture of the dimer-dimer free energy landscape of AXHt-WT and AXHt-I580A systems is provided in Figure 4, where the free energy surface was expressed as a function of two collective variables: the AXH dimer-dimer distance, and the cosine CV.

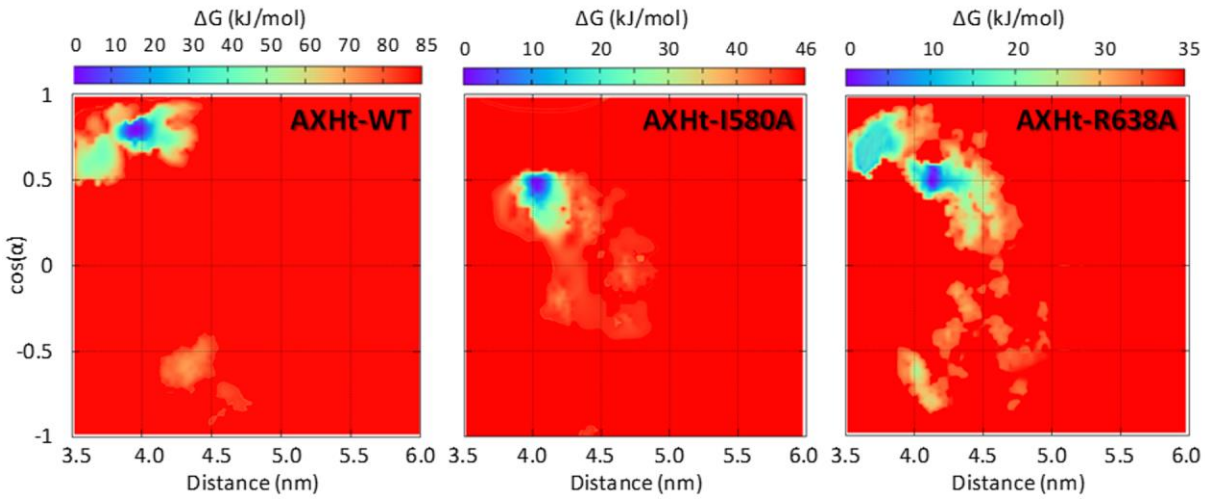

Figure 4. a) Free energy profile (kJ/mol) of the AXHt-WT, AXHt-I580A, and AXHt-R638A molecular systems (b), represented as function of two collective variables: the AXH dimer-dimer distance and the cosine of the angle between vectors connecting two distinct AXH regions per dimer.

A first difference between the two systems concerns the dimer-dimer binding free energy. In detail, AXHt-WT is characterized by the highest binding affinity ($\Delta G_{AXHt\text{-}WT}$=85 kJ/mol; $\Delta G_{AXHt\text{-}I580A}$=46 kJ/mol, Table 1).

Table 1. Tetramer binding affinity values estimated in the present work and compared with a recent experimental work reporting the experimental tetramer percentage in solution [18].

Molecular System	Tetramer ΔG [kJ/mol]	Exp.Tetramer %
AXH-WT	85 ± 3	26 % (18)
AXH-I580A	46 ± 2	8 % (18)
AXH-R638A	35 ± 3	//

Therefore, the I580 alanine substitution results in a lower energetic cost for the dimer-dimer unbinding. This interesting result is in agreement with recent experimental findings [18] demonstrating that the I580 mutation leads to a significant reduction of AXH tetramer percentage in solution (Table 1). Moreover, a difference between the first binding pose can be noticed comparing the cosine CV value corresponding to the deepest energy well in case of AXHt-WT ($\cos(\alpha)_{WT}$=0.8) and the AXHt-I580A ($\cos(\alpha)_{I580A}$=0.5). This result in agreement with Classical MD outcome (Figure 2, Figure 3), indicates a relative rotation between dimers AB and CD as a consequence of I580 mutation, lowering the energetic cost of the dimer-dimer unbinding (Table 1).

Summarizing, from our findings and in agreement with a recent study [18], there is evidence that the I580 mutation affects the dimer-dimer free energy landscape in terms of binding affinity and binding pose. Based on the results of this study, we conjecture this mechanism significantly driven by the destabilization of the R638 residue. To further test this hypothesis, we performed classical MD and metadynamics simulation by replacing the native R638 residues with Alanine (AXHt-R638A), instead of mutating the I580. The results, reported in Figure 4, clearly show that Arginine substitution of R638 dramatically reduces the binding affinity ($\Delta G_{AXHt\text{-}R638A}$=35 kJ/mol) if compared with AXHt-WT and AXHt-I580A (Table 1). Moreover, the comparison between the

cosine CV value corresponding to the deepest energy well in case of AXHt-I580A and AXHt-R638A simulation ($\cos(\alpha)_{I580A}=\cos(\alpha)_{R638A}=0.5$) demonstrate that both molecular systems are characterized by similar binding poses (Figure 4). This outcome provides a convincing evidence on the importance of R638 as the key player in AXH tetramer stability.

Discussion

The present study is mainly focused on the protein-protein interactions driving the AXH tetramer stability, which is thought to play a role in the self-association process of full-length ATX1 and amyloid fibril formation [15]. Previous experimental studies have demonstrated the presence of monomers, dimers, and tetramers in solution [18]. Moreover, the structural consequence of selected mutations, designed to disrupt specific intermolecular interfaces, was analyzed in order to identify residues, which are mainly responsible for determining the monomer/dimer/tetramer equilibrium [18]. Experimental studies have shown that tetramer population was noticeably reduced by I580 mutation, demonstrating that I580 plays an important role in mediating the AXH self-association [18]. However, it was unclear how a centrally located residue in the monomer-monomer interface can affect the tetramer formation mechanism. In this regard, the lack of clear knowledge of the AXH species present in solution makes experimental, more quantitative analysis (i.e., an estimate of the dissociation constants) of the systems very challenging [18]. In this connection, computational approaches have demonstrated to be effective in predicting physical-chemical properties of biomolecular systems [11,40–52], in particular the effect of amino acid mutations on protein-protein [10,20,53] and protein-substrate [54,55] interactions, allowing the free energy estimation corresponding to individual residue substitutions.

In the present work we used classical MD and metadynamics to investigate the structural and dynamic consequences of the I580 mutation, by applying the Principal Component Analysis (PCA) which has already demonstrated to be able to elucidate the large-scale and low-frequency modes mainly related to the AXH conformational changes in monomeric [19] and dimeric [20] form. Here we demonstrated that I580 mutation on AXH dimer leads to the destabilization of the N-terminal tail. Moreover, we observed that the residue R638, spatially close to the fluctuating N-terminal tail, is characterized by a high degree of conformational flexibility (Figure 1). This is an important molecular event, considering that the MD simulation of the wild-type AXH tetramer has demonstrated the non-covalent interaction between the guanidinium groups and the backbone carbonyl oxygens of residues R638B and R638C (Figure 3). Moreover, a less stable interaction between R638B and R638C was observed in case of I580 mutation on AXH tetramer, suggesting a possible explanation for the role played by a centrally located residue in the monomer-monomer interface in reducing the AXH tetramer stability. Starting from the well-established observation that the AXH domain of ATX1 adopts different topologies leading to the asymmetry of monomer-monomer interface [4,5,18–20,56], we hypothesized that the overall tetramer topology may be dependent on the structural fluctuation of the AXH dimer caused by single-point mutation.

To provide further insight into this issue, we applied the metadynamics to estimate the free energy landscape governing the tetramer formation process in case of wilt-type and mutated AXH tetramer system. We observed that I580 alanine substitution resulted in a decreased binding free energy, lowering the energetic cost for the dimer-dimer unbinding. Those findings are in agreement with experimental observations [18] that I580 mutation leads to a significant reduction of AXH tetramer percentage in solution (Table 1). More interestingly, the simulations performed in this study shed light on the importance that the hydrogen bond between R638B and R638C has in driving the

dimer-dimer unbinding event. The effect of R638 conformational instability because of I580 protein mutation leads to a different protein-protein detachment pathway, lowering the energetic cost of the dimer-dimer unbinding (Figure 4). A proof of evidence for this mechanism was provided by the dramatic reduction of binding affinity caused by the replacement of R638 residues with Alanine, and hence demonstrating the importance of R638 residue in driving the AXH tetramer stability (Figure 4).

Taken together, these findings suggest that residue R638 plays a key role in AXH tetramer stability, and candidates to be the target for future experimental designs of ATX1 mutations able to reduce the phenomenon of self-association of full-length ATX1, that leads to amyloid fibril formation and, ultimately, to neurodegenerative disease.

Conclusions

Outcomes of the present study may be of relevance in the field of SCA1 research with particular focus on AXH aggregation mechanism. The R638 residue, identified as mainly responsible for dimer-dimer interaction, may be considered for further *ad hoc* experimental tests, aimed at: i) validating the results presented in this paper and ii) elucidating disease-causing aggregation mechanism.

Acknowledgement

This work was supported by a grant from the Swiss National Supercomputing Centre (CSCS).

Author Contributions

GG, and MAD conceived the research.

GG and MAD, did the molecular dynamics simulations.
GG, UM, AD, JAT, and MAD analyzed and rationalized the data.
All authors wrote the paper and critically commented to the manuscript.

All authors read and approved the final manuscript.

Competing Interests

The authors declare no competing interests

References

1. Zoghbi, H. Y.; Orr, H. T. Pathogenic mechanisms of a polyglutamine-mediated neurodegenerative disease, Spinocerebellar ataxia type 1. *J. Biol. Chem.* 2009, *284*, 7425–7429.
2. Saunders, H. M.; Bottomley, S. P. Multi-domain misfolding: Understanding the aggregation pathway of polyglutamine proteins. *Protein Eng. Des. Sel.* 2009, *22*, 447–451.
3. de Chiara, C.; Giannini, C.; Adinolfi, S.; de Boer, J.; Guida, S.; Ramos, A.; Jodice, C.; Kioussis, D.; Pastore, A. The AXH module: an independently folded domain common to ataxin-1 and HBP1. *FEBS Lett.* **2003**, *551*, 107–112, doi:10.1016/S0014-5793(03)00818-4.
4. de Chiara, C.; Menon, R. P.; Adinolfi, S.; de Boer, J.; Ktistaki, E.; Kelly, G.; Calder, L.; Kioussis, D.; Pastore, A. The AXH domain adopts alternative folds the solution structure of HBP1 AXH. *Structure* **2005**, *13*, 743–53, doi:10.1016/j.str.2005.02.016.
5. Chen, Y. W. Y. W.; Allen, M. D.; Veprintsev, D. B.; Löwe, J.; Bycroft, M. The Structure of the AXH Domain of Spinocerebellar Ataxin-1. *J. Biol. Chem.* **2003**, *279*, 3758–3765, doi:10.1074/jbc.M309817200.
6. de Chiara, C.; Pastore, A. Polyglutamine Diseases and Neurodegeneration: The Example of Ataxin-1. In *Supramolecular Structure and Function 10*; Springer Netherlands: Dordrecht, 2011; pp. 87–99.
7. Nicastro, G.; Todi, S. V; Karaca, E.; Bonvin, A. M. J. J.; Paulson, H. L.; Pastore, A. Understanding the role of the Josephin domain in the PolyUb binding and cleavage properties of ataxin-3. *PLoS One* **2010**, *5*, e12430, doi:10.1371/journal.pone.0012430.
8. Masino, L.; Nicastro, G.; De Simone, A.; Calder, L.; Molloy, J.; Pastore, A. The Josephin domain determines the morphological and mechanical properties of ataxin-3 fibrils.

Biophys. J. **2011**, *100*, 2033–2042, doi:10.1016/j.bpj.2011.02.056.

9. Masino, L.; Nicastro, G.; Calder, L.; Vendruscolo, M.; Pastore, A. Functional interactions as a survival strategy against abnormal aggregation. *FASEB J.* **2011**, *25*, 45–54, doi:10.1096/fj.10-161208.
10. Deriu, M. A.; Grasso, G.; Licandro, G.; Danani, A.; Gallo, D.; Tuszynski, J. A.; Morbiducci, U. Investigation of the Josephin Domain Protein-Protein Interaction by Molecular Dynamics. *PLoS One* **2014**, *9*, e108677, doi:10.1371/journal.pone.0108677.
11. Apicella, A.; Soncini, M.; Deriu, M. A.; Natalello, A.; Bonanomi, M.; Dellasega, D.; Tortora, P.; Regonesi, M. E.; Casari, C. S. A hydrophobic gold surface triggers misfolding and aggregation of the amyloidogenic Josephin domain in monomeric form, while leaving the oligomers unaffected. *PLoS One* **2013**, *8*, e58794, doi:10.1371/journal.pone.0058794.
12. Grasso, G.; Tuszynski, J. A.; Morbiducci, U.; Licandro, G.; Danani, A.; Deriu, M. A. Thermodynamic and kinetic stability of the Josephin Domain closed arrangement: evidences from replica exchange molecular dynamics. *Biol. Direct* **2017**, *12*, 2, doi:10.1186/s13062-016-0173-y.
13. Deriu, M. A.; Grasso, G.; Tuszynski, J. A.; Gallo, D.; Morbiducci, U.; Danani, A. Josephin Domain Structural Conformations Explored by Metadynamics in Essential Coordinates. *PLOS Comput. Biol.* **2016**, *12*, e1004699, doi:10.1371/journal.pcbi.1004699.
14. Kuiper, E. F. E.; de Mattos, E. P.; Jardim, L. B.; Kampinga, H. H.; Bergink, S. Chaperones in Polyglutamine Aggregation: Beyond the Q-Stretch. *Front. Neurosci.* **2017**, *11*, doi:10.3389/fnins.2017.00145.
15. De Chiara, C.; Menon, R. P.; Dal Piaz, F.; Calder, L.; Pastore, A. Polyglutamine is not all: The functional role of the AXH domain in the ataxin-1 protein. *J. Mol. Biol.* **2005**, *354*,

883–893, doi:10.1016/j.jmb.2005.09.083.

16. Emamian, E. S.; Kaytor, M. D.; Duvick, L. A.; Zu, T.; Tousey, S. K.; Zoghbi, H. Y.; Clark, H. B.; Orr, H. T. Serine 776 of ataxin-1 is critical for polyglutamine-induced disease in SCA1 transgenic mice. *Neuron* **2003**, *38*, 375–387, doi:10.1016/S0896-6273(03)00258-7.

17. Tsuda, H.; Jafar-Nejad, H.; Patel, A. J.; Sun, Y.; Chen, H. K.; Rose, M. F.; Venken, K. J. T.; Botas, J.; Orr, H. T.; Bellen, H. J.; Zoghbi, H. Y. The AXH domain of ataxin-1 mediates neurodegeneration through its interaction with Gfi-1/senseless proteins. *Cell* **2005**, *122*, 633–644, doi:10.1016/j.cell.2005.06.012.

18. De Chiara, C.; Rees, M.; Menon, R. P.; Pauwels, K.; Lawrence, C.; Konarev, P. V.; Svergun, D. I.; Martin, S. R.; Chen, Y. W.; Pastore, A. Self-assembly and conformational heterogeneity of the AXH domain of ataxin-1: An unusual example of a chameleon fold. *Biophys. J.* **2013**, *104*, 1304–1313, doi:10.1016/j.bpj.2013.01.048.

19. Grasso, G.; Deriu, M. A.; Tuszynski, J. A.; Gallo, D.; Morbiducci, U.; Danani, A. Conformational fluctuations of the AXH monomer of Ataxin-1. *Proteins Struct. Funct. Bioinforma.* **2016**, *84*, 52–59, doi:10.1002/prot.24954.

20. Deriu, M. A.; Grasso, G.; Tuszynski, J. A.; Massai, D.; Gallo, D.; Morbiducci, U.; Danani, A. Characterization of the AXH domain of Ataxin-1 using enhanced sampling and functional mode analysis. *Proteins Struct. Funct. Bioinforma.* **2016**, *84*, 666–673, doi:10.1002/prot.25017.

21. Menon, R. P.; Soong, D.; de Chiara, C.; Holt, M.; McCormick, J. E.; Anilkumar, N.; Pastore, A. Mapping the self-association domains of ataxin-1: identification of novel non overlapping motifs. *PeerJ* **2014**, *2*, e323, doi:10.7717/peerj.323.

22. Bussi, G.; Donadio, D.; Parrinello, M. Canonical sampling through velocity rescaling. *J.*

Chem. Phys. **2007**, *126*, 14101, doi:10.1063/1.2408420.

23. Berendsen, H. J. C.; Postma, J. P. M.; Van Gunsteren, W. F.; DiNola, A.; Haak, J. R. Molecular dynamics with coupling to an external bath. *J. Chem. Phys.* **1984**, *81*, 3684–3690, doi:10.1063/1.448118.

24. Nosé, S.; Klein, M. L. Constant pressure molecular dynamics for molecular systems. *Mol. Phys.* **1983**, *50*, 1055–1076, doi:10.1080/00268978300102851.

25. Parrinello, M.; Rahman, A. Polymorphic transitions in single crystals: A new molecular dynamics method. *J. Appl. Phys.* **1981**, *52*, 7182–7190, doi:10.1063/1.328693.

26. Hornak, V.; Abel, R.; Okur, A.; Strockbine, B.; Roitberg, A.; Simmerling, C. Comparison of multiple Amber force fields and development of improved protein backbone parameters. *Proteins* **2006**, *65*, 712–25, doi:10.1002/prot.21123.

27. Lindorff-Larsen, K.; Piana, S.; Palmo, K.; Maragakis, P.; Klepeis, J. L.; Dror, R. O.; Shaw, D. E. Improved side-chain torsion potentials for the Amber ff99SB protein force field. *Proteins* **2010**, *78*, 1950–8, doi:10.1002/prot.22711.

28. Jorgensen, W. L.; Chandrasekhar, J.; Madura, J. D.; Impey, R. W.; Klein, M. L. Comparison of simple potential functions for simulating liquid water. *J. Chem. Phys.* **1983**, *79*, 926, doi:10.1063/1.445869.

29. Lindorff-Larsen, K.; Maragakis, P.; Piana, S.; Eastwood, M. P.; Dror, R. O.; Shaw, D. E. Systematic validation of protein force fields against experimental data. *PLoS One* **2012**, *7*, e32131, doi:10.1371/journal.pone.0032131.

30. Bonomi, M.; Branduardi, D.; Bussi, G.; Camilloni, C.; Provasi, D.; Raiteri, P.; Donadio, D.; Marinelli, F.; Pietrucci, F.; Broglia, R. A.; Parrinello, M. PLUMED: A portable plugin for free-energy calculations with molecular dynamics. *Comput. Phys. Commun.* **2009**, *180*,

1961–1972, doi:10.1016/j.cpc.2009.05.011.

31. Tribello, G. A.; Bonomi, M.; Branduardi, D.; Camilloni, C.; Bussi, G. PLUMED 2: New feathers for an old bird. *Comput. Phys. Commun.* **2014**, *185*, 604–613, doi:10.1016/j.cpc.2013.09.018.

32. Hess, B.; Kutzner, C.; van der Spoel, D.; Lindahl, E. GROMACS 4: Algorithms for Highly Efficient, Load-Balanced, and Scalable Molecular Simulation. *J. Chem. Theory Comput.* **2008**, *4*, 435–447, doi:10.1021/ct700301q.

33. Humphrey, W.; Dalke, A.; Schulten, K. VMD: visual molecular dynamics. *J. Mol. Graph.* **1996**, *14*, 33–8, 27–8, doi:10.1016/0263-7855(96)00018-5.

34. Maisuradze, G. G.; Liwo, A.; Scheraga, H. a Principal component analysis for protein folding dynamics. *J. Mol. Biol.* **2009**, *385*, 312–29, doi:10.1016/j.jmb.2008.10.018.

35. Barducci, A.; Bonomi, M.; Parrinello, M. Metadynamics. *Wiley Interdiscip. Rev. Comput. Mol. Sci.* **2011**, *1*, 826–843, doi:10.1002/wcms.31.

36. Laio, A.; Parrinello, M. Escaping free-energy minima. *Proc. Natl. Acad. Sci. U. S. A.* **2002**, *99*, 12562–12566, doi:10.1073/pnas.202427399.

37. Laio, A.; Gervasio, F. L. Metadynamics: a method to simulate rare events and reconstruct the free energy in biophysics, chemistry and material science. *Reports Prog. Phys.* 2008, *71*, 126601.

38. Granata, D.; Camilloni, C.; Vendruscolo, M.; Laio, A. Characterization of the free-energy landscapes of proteins by NMR-guided metadynamics. *Proc. Natl. Acad. Sci. U. S. A.* **2013**, *110*, 6817–22, doi:10.1073/pnas.1218350110.

39. Bonomi, M.; Barducci, A.; Parrinello, M. Reconstructing the equilibrium boltzmann distribution from well-tempered metadynamics. *J. Comput. Chem.* **2009**, *30*, 1615–1621,

doi:10.1002/jcc.21305.

40. Rui, H.; Artigas, P.; Roux, B. The selectivity of the Na + /K + -pump is controlled by binding site protonation and self-correcting occlusion. *Elife* **2016**, *5*, doi:10.7554/eLife.16616.

41. Burnley, B. T.; Afonine, P. V; Adams, P. D.; Gros, P. Modelling dynamics in protein crystal structures by ensemble refinement. *Elife* **2012**, *1*, doi:10.7554/eLife.00311.

42. Paciello, G.; Acquaviva, A.; Ficarra, E.; Deriu, M. A.; Macii, E. A molecular dynamics study of a miRNA:mRNA interaction. *J. Mol. Model.* **2011**, *17*, 2895–906, doi:10.1007/s00894-011-0991-x.

43. Gentile, F.; Deriu, M.; Licandro, G.; Prunotto, A.; Danani, A.; Tuszynski, J. Structure Based Modeling of Small Molecules Binding to the TLR7 by Atomistic Level Simulations. *Molecules* **2015**, *20*, 8316–8340, doi:10.3390/molecules20058316.

44. Deriu, M. A.; Popescu, L. M.; Ottaviani, M. F.; Danani, A.; Piticescu, R. M. Iron oxide/PAMAM nanostructured hybrids: combined computational and experimental studies. *J. Mater. Sci.* **2016**, *51*, 1996–2007, doi:10.1007/s10853-015-9509-8.

45. Havelka, D.; Deriu, M. A.; Cifra, M.; Kučera, O. Deformation pattern in vibrating microtubule: Structural mechanics study based on an atomistic approach. *Sci. Rep.* **2017**, *7*, doi:10.1038/s41598-017-04272-w.

46. Deriu, M. A.; Bidone, T. C.; Mastrangelo, F.; Di Benedetto, G.; Soncini, M.; Montevecchi, F. M.; Morbiducci, U. Biomechanics of actin filaments: A computational multi-level study. *J. Biomech.* **2011**, *44*, 630–636, doi:10.1016/j.jbiomech.2010.11.014.

47. Deriu, M. A.; Enemark, S.; Soncini, M.; Montevecchi, F. M.; Redaelli, A. Tubulin: from atomistic structure to supramolecular mechanical properties. *J. Mater. Sci.* **2007**, *42*, 8864–8872, doi:10.1007/s10853-007-1784-6.

48. Deriu, M. A.; Shkurti, A.; Paciello, G.; Bidone, T. C.; Morbiducci, U.; Ficarra, E.; Audenino, A.; Acquaviva, A. Multiscale modelling of cellular actin filaments: From atomistic molecular to coarse grained dynamics. *Proteins Struct. Funct. Bioinforma.* **2012**, *80*, 1598–609, doi:10.1002/prot.24053.

49. Soncini, M.; Vesentini, S.; Ruffoni, D.; Orsi, M.; Deriu, M. A.; Redaelli, A. Mechanical response and conformational changes of alpha-actinin domains during unfolding: A molecular dynamics study. *Biomech. Model. Mechanobiol.* **2007**, *6*, 399–407, doi:10.1007/s10237-006-0060-z.

50. Karplus, M.; McCammon, J. A. Molecular dynamics simulations of biomolecules. *Nat. Struct. Biol.* **2002**, *9*, 646–652, doi:10.1038/nsb0902-646.

51. Deriu, M. A.; Soncini, M.; Orsi, M.; Patel, M.; Essex, J. W.; Montevecchi, F. M.; Redaelli, A. Anisotropic elastic network modeling of entire microtubules. *Biophys. J.* **2010**, *99*, 2190–2199, doi:10.1016/j.bpj.2010.06.070.

52. Kuzmanic, A.; Sutto, L.; Saladino, G.; Nebreda, A. R.; Gervasio, F. L.; Orozco, M. Changes in the free-energy landscape of p38α MAP kinase through its canonical activation and binding events as studied by enhanced molecular dynamics simulations. *Elife* **2017**, *6*, doi:10.7554/eLife.22175.

53. Joseph, P. R. B.; Poluri, K. M.; Gangavarapu, P.; Rajagopalan, L.; Raghuwanshi, S.; Richardson, R. M.; Garofalo, R. P.; Rajarathnam, K. Proline substitution of dimer interface ??-strand residues as a strategy for the design of functional monomeric proteins. *Biophys. J.* **2013**, *105*, 1491–1501, doi:10.1016/j.bpj.2013.08.008.

54. Gu, Z.; Yang, Z.; Chong, Y.; Ge, C.; Weber, J. K.; Bell, D. R.; Zhou, R. Surface Curvature Relation to Protein Adsorption for Carbon-based Nanomaterials. *Sci. Rep.* **2015**, *5*, 10886,

doi:10.1038/srep10886.

55. Grasso, G.; Deriu, M. A.; Prat, M.; Rimondini, L.; Vernè, E.; Follenzi, A.; Danani, A. Cell Penetrating Peptide Adsorption on Magnetite and Silica Surfaces: A Computational Investigation. *J. Phys. Chem. B* **2015**, *119*, 8239–8246, doi:10.1021/jp512782e.

56. de Chiara, C.; Pastore, A. Kaleidoscopic protein–protein interactions in the life and death of ataxin-1: new strategies against protein aggregation. *Trends Neurosci.* **2014**, *37*, 211–218, doi:10.1016/j.tins.2014.02.003.

57. Ziebarth, J.; Wang, Y. Molecular Dynamics Simulations of DNA-Polycation Complex Formation. *Biophys. J.* **2009**, *97*, 1971–1983, doi:10.1016/j.bpj.2009.03.069.

Figure Legends

Figure 1. a) Visual inspection of the AXH-WT conformational arrangement at the equilibrium (left). The Root Mean Square Fluctuation (RMSF) is reported in the right panel and represented on the protein 3D structure (center). b) Visual inspection of the AXH-I580A conformational arrangement at the equilibrium (left). The Root Mean Square Fluctuation (RMSF) is reported in the right panel and represented on the protein 3D structure (center).

Figure 2. Backbone RMSD throughout the overall MD simulation for wild type (grey) and mutated protein (brown). b) Visual inspection of the molecular systems at the equilibrium in case of AXHt-WT (I) and AXHt-I580A system (II). c) Scheme illustrating the main structural modifications characterized by a relative rotation between dimers AB and CD.

Figure 3. (a) RDF of the amine nitrogen atoms of guanidinium group with respect the backbone carbonyl oxygens of the interacting arginine residue. Only R638B and R638C are considered for the calculation. Two different peaks at 2.8 Å and 4.7 Å can be identified. The first peak is related to the primary interaction resulting from the hydrogen bond between the amine hydrogen atoms and the backbone oxygen, while the second peak indicates the water-mediated hydrogen bonding [57]. The hydrogen bonds between the R638B and R638C residues are also represented in (b) and (c).

Figure 4. a) Free energy profile (kJ/mol) of the AXHt-WT, AXHt-I580A, and AXHt-R638A molecular systems (b), represented as function of two collective variables: the AXH dimer-dimer distance and the cosine of the angle between vectors connecting two distinct AXH regions per dimer.

Table Legends

Table 1. Tetramer binding affinity values estimated in the present work and compared with a recent experimental work reporting the experimental tetramer percentage in solution [18].

View publication stats